Published in final edited form as:
Exp Cell Res. 2011 April 1; 317(6): 691–705. doi:10.1016/j.yexcr.2011.01.008.

The cation channel mucolipin-1 is a bifunctional protein that facilitates membrane remodeling via its serine lipase domain

Janice M. LaPlante[*], **John L. Falardeau**[+], **Edward M. Brown**[*], **Susan A. Slaugenhaupt**[+], and **Peter M. Vassilev**[*]

[*]Division of Endocrinology, Diabetes and Hypertension and Membrane Biology Program, Department of Medicine, Brigham & Women's Hospital and Harvard Medical School, Boston, Massachusetts 02115

[+]Center for Human Genetic Research, Massachusetts General Hospital and Harvard Medical School, Boston, Massachusetts 02115

Abstract

Phospholipase modulators have been shown to affect the topology of lipid bilayers and the formation of tubulo-vesicular structures, but the specific endogenous phospholipases involved have yet to be identified. Here we show that TRPML1 (MLN1), a Ca^{2+}-permeable channel contributes to membrane remodeling through a serine-lipase consensus domain, and thus represents a novel type of bifunctional protein. Remarkably, this serine lipase active site determines the ability of MLN1 to generate tubulo-vesicular extensions in mucolipin-1-expressing oocytes, human fibroblasts and model membrane vesicles. Our demonstration that MLN1 is involved in membrane remodeling and the formation of extensions suggests that it may play a role in the formation of cellular processes linked to the late endosome/lysosome (LE/L) pathway. MLN1 is absent or mutated in patients with mucolipidosis IV (MLIV), a lysosomal disorder with devastating neurological and other consequences. This study provides potential insight into the pathophysiology of MLIV.

Keywords

membrane remodeling; phospholipase; TRPML1; mucolipin; mucolipidosis IV; tubulo-vesicular

INTRODUCTION

In a previous study we established that TRPML1, also known as mucolipin-1, MLN1 or ML1), functions as a novel nonselective cation channel that is permeable to Ca^{2+}, K^{+}, Na^{+} and other cations [1]. The activity of this channel in endosomal [2] and LE/L membranes [3], as well as its dependence on Ca^{2+} [1] have also been characterized. Mutations in

Correspondence should be addressed to: Dr. Janice M. LaPlante, Division of Endocrinology, Diabetes and Hypertension, Department of Medicine, Brigham & Women's Hospital and Harvard Medical School, Boston, MA 02115, Tel: 617-312-0329; FAX: 617-663-6662; jlaplante@rics.bwh.harvard.edu; janice_marie_laplante@yahoo.com.

COMPETING INTERESTS STATEMENT
The authors declare that they have no competing financial interests.

MCOLN1, the gene encoding mucolipin-1 [4-6], cause mucolipidosis IV (MLIV), an autosomal recessive disease that leads to severe cognitive and developmental impairment, psychomotor disturbances and eventual blindness [7]. At the cellular level, the disease is characterized by large inclusions associated with the lysosomal pathways in most cells and tissues [8-12]. Previous reports suggested that, unlike other mucolipidoses, the main cellular phenotype in MLIV is related to a deficiency in LE/L trafficking [12-13] rather than to a defect in lysosomal enzymatic activity. A recent report, however, indicated that a disturbance in lipid hydrolysis and metabolism may also play a role in MLIV [14]. MLN1 contains two di-leucine motifs for LE/L localization [6] but it is also expressed on the plasma membrane, where we characterized its properties on the surface of intact oocytes expressing MLN1 [1]. This expression is apparently due to constitutive lysosomal exocytosis, a ubiquitous phenomenon that has been studied not only in specialized secretory cells but also in a variety of other cell types [15-17]. We have previously shown that the translocation of MLN1 to the plasma membrane is promoted by stimulating lysosomal exocytosis with the Ca^{2+} ionophore, ionomycin, suggesting that MLN1 may play a role in the redistribution of lysosomes and their fusion with the plasma membrane [1,3,18] .

One of the remarkable features of MLN1 is the presence of a consensus sequence for a serine lipase active site on the large loop between the first and second transmembrane domains. We hypothesized that in addition to its potential role as a cation channel, MLN1 may also contribute to cellular lipase activity within the late endosomal pathway or at the cell surface. Its overexpression in oocytes promotes lysosomal exocytosis as well as the formation and extension of tubulo-vesicular structures (TVS). No such structures are generated in oocytes that overexpress MLN1 with a mutated serine lipase active site (SL), and the exocytotic process is less efficient in these oocytes in comparison to the wild type (WT)-MLN1-expressing oocytes. We considered the possibility that this serine lipase site is functional and may play a role in the mechanism of action of MLN1 on LE/L exocytosis and membrane reshaping.

Here we show that a soluble fragment corresponding to the intralumenal loop of MLN1 is sufficient to promote phospholipase activity in a model membrane system, but that mutation of the serine lipase site disrupts these activities. We also present evidence of a plasma membrane reshaping activity in wild type human fibroblasts comparable to that which we observed in oocytes, activity that is reduced in fibroblasts from MLIV patients. This activity can be rescued in MLIV fibroblasts by transfection with WT-MLN1 cDNA, but not with two separate cDNAs with point mutations in the serine lipase site, one of which is a naturally occurring mutation from an MLIV patient [19]. Our results suggest that the loss of MLN1's serine lipase function may be associated with impaired membrane trafficking/ remodeling, a phenotype that could potentially contribute to the pathogenesis of the disease.

MATERIALS AND METHODS

Mucolipin-1 expression constructs

MCOLN1 cDNA (Gene Bank Accession Number AF287269) was synthesized by reverse transcription of total RNA from normal human fibroblasts. The 2025 bp sequence includes a 1740 bp open reading frame. The cDNA was cloned into the mammalian expression vector, pSV-Sport1 (Gibco BRL). C-terminal and N-terminal GFP fusion constructs were generated by the in-frame insertions of the GFP domain from pEGFP-C1 into the pSV-MLN1 construct. No differences in any of the activities and localization were observed between the C- and N-terminal GFP expression constructs nor did they differ from the wild type protein.

Site-directed mutagenesis

The procedure was performed on the MLN1-GFP/pSPORT cDNA vectors using the Stratagene Quick Change Mutagenesis kit (Invitrogen). To form the SL mutation, the oligonucleotide primers: 5′CTTCCTGCTGGGCGGTGGAGACGGAGCGGATG-3′ and 5′-CATCCGCTCCGTCTCCACCGCCCAGCAGGAAG-3′, were used to change the amino acid sequence in the serine lipase site from “GYSDG” to “GGGDG”. To form the L106P mutation, the oligonucleotide primers:. 5′-CCGACACCTCTTCCCGCTGGGCTACTCGG -3′ and 5′-CCGAGTAGCCCAGCGGGAAGAGGTGTCGG-3′ were used [19]. The F465L mutation in MLN1-GFP/pSPORT cDNA vectors was obtained from Dr. Mei Sun (Developmental and Metabolic Neurology Branch, NIH).

Preparation of the MLN1-lipase fusion protein

A cDNA fragment corresponding to the lumenal domain between the first and second transmembrane domains of WT or SL-MLN1 (Arg_{94}-Arg_{298}) was synthesized by PCR using the primers: F-5′-CACCCGGGAAGAGAACACCATCG-3′ and R-5′-TTACCGGAAGCTGTTGTCTCC-3′. The fragments were cloned into the prokaryotic expression vector, pET100/D-TOPO, which contains a 6xHis domain for purification on a nickel column and an X-press epitope for identification by Western blot. A fusion protein was produced using an *in vitro* translation system or a bacterial expression system or, with similar results, in the model membrane systems described above. *In vitro* expression was achieved using the PROTEINscript™-PRO E. coli lysate system (Ambion). For higher yields, the constructs were transformed into E. coli strain BL21-DE3, expressed and purified using the Pro-Bond Purification System (Invitrogen) according to the manufacturer’s instructions. A semi-purified fusion protein was identified in the enriched extracts by standard Western blotting techniques using an antibody raised against the X-press epitope (Invitrogen).

Oocyte preparation and expression of MLN1 in oocytes

Capped RNA was synthesized from linearized pSV-Sport-1 templates using the mMessage mMachine *In Vitro* Transcription Kit (Ambion) and modified with the Poly(A) Tailing Kit (Ambion). Oocytes at stage V-VI were harvested from *Xenopus laevis* and defolliculated by treating them for 2 hours at 18°C with 2 mg/ml collagenase in a Ca^{2+}-free Barth’s solution. The oocytes were injected, on the same day (at least 4 hours after defolliculation) or on the following day, with 50 nl H_2O containing 50 ng cRNA of MLN1 or of the SL-MLN1 mutant. Equal amounts of H_2O were injected into control oocytes. Injected oocytes were incubated at 14-18°C in Barth’s solution containing 0.5 mM $CaCl_2$.

MLN1 expression and LE/L distribution

The localization of MLN1 was visualized in oocytes by bright field microscopy or GFP epifluorescence. Images were collected and analyzed using a Zeiss inverted microscope with a fluorescence attachment, Optronics digital camera and ImagePro Plus Software (Media Cybernetics) programs.

Fluorescence measurements of enzyme activities in oocytes

Phospholipase activity—The method for assessment of phospholipase activity in LE/L-containing oocyte extracts was based on measuring the fluorescence of the cleavage products generated from the enzyme substrates, bis-BODIPY FL C11-PC and Bodipy FL C5–HPC probes (Molecular Probes), as previously described [20-21]. These probes were used at concentrations of 0.3 or 0.35 μM, respectively. The main assay solution was 100 mM Na acetate and the incubation was usually for 2 hr at 37°C. The reaction was stopped by a 10-fold dilution of the assay solution. Fluorescence intensity for both probes was measured

at 495 nm excitation and 520 nm emission. The standard curve was linear with bis-BODIPY FL C11-PC concentration up to 4uM and that with Bodipy FL C5-HPC concentration up to 4.5 μM. The use of TLC and other procedures related to the lipase activity in LE/L-containing oocyte extracts are described in detail below in the experimental section for the model membrane system.

Lysosomal enzyme release assay—The method for measuring the release of the lysosomal enzyme, N-acetyl-beta-D-glucosaminidase (NAG) from whole oocytes was based on measuring the fluorescent product from the enzyme substrate, 4-methyl-umbelliferyl-N-acetyl-beta-D-glucosaminide, as previously described [16-17,22]. The amount of NAG released for each condition is expressed as percentage of the total content of NAG in the cells determined after their lysis using 0.1% Triton X-100. In control studies on cellular viability, no substantial changes in lactate dehydrogenase activity were observed during treatment with ionomycin, showing that the changes in NAG release cannot be attributed to cellular toxicity.

Subcellular preparations and reconstitution of MLN1 in membrane vesicles

The procedures were carried out as described in previous studies [3,23-25]. The oocytes were gently triturated using small pipette tips followed by homogenization with Teflon-coated pestle in a solution containing in mM: 250 sucrose, 1 EGTA, 2 MgCl2, and 10 Hepes (pH 7.4). Homogenates were centrifuged for 5 minutes at 700 × g. The supernatant was centrifuged for 10 minutes at 1,100 x g and the resulting supernatant was used to obtain the LE/L fractions by additional high speed centrifugations. A combination of techniques for fusing LE/L fractions with large liposomes [23] and for forming patch-clamp bilayers [24-25] from these vesicles was used for reconstitution of MLN1 activities. The liposomes were prepared from asolectin or brain phospholipids (2 mg/ml) by three cycles of freezing at −80°C and thawing at 23°C, followed by partial dehydration in a vacuum dessicator for 30 min and rehydration for 2 h. The LE/L fractions were added to the liposomes during the rehydration procedure (usually 15 min after the beginning of the rehydration) to maximize the effectiveness of the reconstitution process.

Liposome vesicle membrane reshaping and lipase activity in the model membrane system

The PLA assay was carried out by incubating liposomes (0.5 μg/μl phospholipid; 1.5 μg/ml Bodipy FL C_5-HPC) with the WT- or SL-MLN1 *in vitro* translated fragments (1:25 –1:100 final dilution) at 37°C for 2 hr in 100 mM Na acetate. The reaction was stopped by addition of hexane/ether (1:1, v/v) or CH_3OH:$CHCl_3$ (1:2, v/v). The organic fractions were removed and separated by TLC using solvent systems that contained hexane, ether and acetic acid or $CHCl_3$/CH_3OH:/NH_4OH/H_2O (65:35:2.5:2.5 by volume). The PLA activity was estimated by measuring the fluorescence intensity in the different spots containing the cleaved free fatty acids and other products of the enzymatic reaction. Varying amounts of fatty acids labeled with the same fluorescent markers as the phospholipid substrates were co-chromatographed to prepare standard calibration curves. The *in vitro* translated serine lipase motif-containing protein fragments described above were synthesized with the PROTEINscriptTM-PRO E. coli lysate transcription/translation system (Ambion), using 0.5 g DNA plasmid template in a reaction volume of 50 μl. The rate of generation of each fluorescent product as a result of the cleavage of each substrate during the incubation period was expressed in nanomoles/h. The fluorescence intensities of the spots containing enzymatically cleaved free fluorescent fatty acids and those of the spots containing the standard fluorescent free fatty acids utilized at different concentrations for calibration were compared. The substrates and the products were all obtained from Molecular Probes. The following substrates were used: 1,2-bis-(4,4-difluoro-5,7-dimethyl-4-bora-3a,4a-diaza-*s*-indacene-3-undecanoyl)-*sn*-glycero-3-phosphocholine (bis-Bodipy FL C_{11}-PC); 2-(4,4-

difluoro-5,7-dimethyl-4-bora-3a,4a-diaza-*s*-indacene-3-pentanoyl)-1-hexadecanoyl-*sn*-glycero-3-phosphocholine (beta-Bodipy FL C_5-HPC); and *N*-((6-(2,4-dinitrophenyl)amino)hexanoyl)-2-(4,4-difluoro-5,7-dimethyl-4-bora-3a,4a-diaza-*s*-indacene-3-pentanoyl-1-hexcadecanoyl-*sn*glycero-3-phosphoethanplamine, triethylammonium salt (PED6). The products were the following: 4,4-difluoro-5,7-dimethyl-4-bora-3a,4a-diaza-*s*-indacene-3-undecanoic acid (Bodipy FL C_{11}), which is the product from the cleavage of bis-Bodipy FL C_{11}-PC; and 4,4-difluoro-5,7-dimethyl-4-bora-3a,4a-diaza-*s*-indacene-3-pentanoic acid (Bodipy FL C_5), which is the product from the cleavage of both beta-Bodipy FL C_5-HPC and PED6. The liposomes for the membrane remodeling experiments were prepared from asolectin or brain phospholipids (Type I, Folch fraction I, Sigma) (1mg/ml) by three cycles of freezing at −80°C and thawing at 23°C followed by partial dehydration in a vacuum dessicator for 30 min and rehydration for 2 h. Sulforhodamine-PE or NBD-PS (1μg/ml) were used as fluorescent probes to stain the liposomal membranes. The liposomes were incubated at 37°C for 2-24 hr in 100 mM Na acetate in the presence or absence of WT- or SL-MLN1 *in vitro* translated fragments (1:25 – 1:100 final dilution), and the number of tubular structures was determined in each of the wells.

Electrophysiological measurements for channel characterization

Patch-clamp methodologies were employed [23-25] for measurement of single channel currents in membrane patches excised from the proteoliposomes after the reconstitution procedure. Patch pipettes were filled with a solution containing in mM (unless otherwise specified): 100 KCl, 0.1 CaCl2, 10 Hepes, pH, 7.5. High resistance seals were employed in the single channel experiments. The currents were measured with an integrating patch-clamp amplifier. Single channel currents were filtered at 3-10 kHz through an 8-pole Bessel filter. The internal solution contained, unless otherwise specified: 100 mM KCl, 0.1 **μM** CaCl2, 10 mM Hepes, and 5 mM EGTA, pH, 7.5.

Data acquisition and analysis

Voltage stimuli were applied and currents digitized (50-200 μs per point) and analyzed using a PC, a Digidata converter, and programs based on pClamp. The probability of channel opening (nPo) was calculated from 1-20 min segments of current records. The Goldman-Hodgkin-Katz (GHK) equation was used to calculate the permeability ratios between Na+ (PNa) and K+ (PK): Erev = RT/F ln [PNa/PK], where Erev is the change in reversal potential measured when K+ is replaced by Na+ in the pipette solution; R, T, and F are the gas constant, absolute temperature, and Faraday constant, respectively.

Statistical analysis

Results are expressed as means ± S.E.M. The statistical analysis was performed using the specialized software package, GraphPad Software Inc. San Diego, CA or Microsoft Excel. The level of statistical significance was defined as $p < 0.05$ and differences were considered significant when p was less than this value.

Characterization of surface membrane vesicles in human fibroblasts

Cell Sources—MLIV primary dermal fibroblasts derived from MLIV patients were used [1]. In this study we used fibroblasts from a patient from Family 50 [6] that is heterozygous for the Ashkenazi Jewish (AJ) minor mutation and a 598-599delCC frameshift, or fibroblasts from patients homozygous for the major AJ mutation (97.33 and 96.73). These mutations have been previously described [4-6], and all result in the complete loss of expression of MLN1. Age-matched normal primary dermal fibroblasts were obtained as

control from the Coriell Cell Repositories. Experiments were performed in fibroblasts between passages 10-30, and results were consistent throughout.

Expression of MLN1 in fibroblasts—The preparation of the MLN1 expression constructs [1] and the protocol for transfection into human primary fibroblasts [18] have been previously described. We verified protein expression from the constructs and localization to the lysosomes. Cells were visualized in multiple z-planes on a Leica SP5 Laser Scanning Confocal microscope. Green fluorescence intensity (GFP expression) was compared to red fluorescence intensity in which acidic organelles of the LE/L pathway were stained with LysoTracker® redDND-99 (Molecular Probes). Results were expressed as the number of green pixels that were present as AND pixels when the green and red images were aligned. Three adjacent images per cell were averaged (n=3 for all constructs).

Characterization of TVS on fibroblasts—Fibroblasts incubated in DMEM/10%FCS/ 5% CO2 were stained with either red CMDiI for 40 min, or greenDiI-C16(3) or red DiI-C16(3) (Molecular Probes, Invitrogen, 5-10 μg/ml), for 1 hrs, chased for 2-3 hr. When calcein was used, beginning 30 min before viewing, 10 μg/ml calcein-AM (Molecular Probes, Invitrogen) was added to the media for 15 min, and subsequently chased in calcein free medium for 15 minutes. Coverslips were inverted into Mattek glass bottomed culture dishes which contained Optimem (Invitrogen), and viewed under laser scanning confocal microscopy (Leica SP5) at 400x magnification under temperature and humidity controlled conditions. Images were analyzed using the CellProfiler image analysis software package (www.cellprofiler.org) [26-27]. TVS protruding from top surface of the cells appeared as oval or bulb-shaped surface vesicles. These vesicles were visualized more clearly when extending downward from the cells on the inverted coverslips. The “Find Edges” algorithm was used to initially identify membrane bounded cell surface objects that stained with the fluorescent C16(3) lipid. These images were converted to binary images and segmented by size, to include objects within the window of 8-20 pixels, corresponding to a range of 3-7.5 μm in diameter. They were subsequently filtered by shape, to exclude objects with an eccentricity ratio >0.85. Filtered images from the multiple planes of the z-stack were overlaid to ensure that each object was counted once and only once. The final image was manually edited to remove artifacts before measuring the total TVS pixel area from each field. The Percent TVS Area was calculated by dividing the TVS Area in a field by the total cellular area within the field. The TVS Ratio was calculated by normalizing the Percent TVS Area values in a sample to the mean value for MLIV cells when comparing untransfected cells, or for MLIV +Vector cells when comparing transfected cells. Each data point represents an average value obtained for an entire field of 10-20 cells. (n) is the number of fields counted over three independent experiments. Data was plotted using Microsoft Excel. Results are expressed as means ± S.E.M. P-values were based on a 2-tailed TTEST, Results were described as significant when $p < 0.05$* and highly significant when $p < 0.01$**.

RESULTS AND DISCUSSION

Formation and extrusion of TVS mediated by overexpression of MLN1

During prolonged observation of oocytes expressing MLN1, we witnessed phenomena that suggested a potential link between the activity of MLN1 and the processes of membrane reshaping and vesiculation. To avoid potential deterioration in the integrity of oocytes, most of our previous electrophysiological studies [1,3] were carried out 2-3 days after injection of the oocytes with MLN1-cRNA. Many oocytes, however, remain viable for extended periods, and when these were examined we noticed an increasing number of tubular and vesicular structures extruding from apparently intact oocytes (Figure 1). These TVS began appearing 3-5 days after injection with MLN1-cRNA, and later there was a dramatic increase in their

numbers. Small vesicular buds or bulb-shaped formations can be seen on the surface of oocytes on days 3-5 (Figure 1a and b), and these protrusions grow into cylindrical and twisted tubular structures by days 6-8 (Figure 1c-e). After 6 days, TVS of various sizes surround the oocytes. Some of them are smaller than 1 μm, while others are 10-30 μm or even larger in diameter (Figure 1d and e). They appear to be pinched off from the tubules that are formed initially or to have been released from the oocyte in a manner analogous to the exocytosis of multi-vesicular bodies. They are similar in shape but larger in size than the exosomal, megavesicular, tubular and other types of TVS [28-30] that are related to LE/L-dependent secretory pathways. TVS were also abundantly formed in MLN1-expressing oocytes treated with actinomycin D, an approach commonly used to distinguish between the activities mediated by exogenously expressed proteins and those arising from endogenous channels or other proteins in *Xenopus* oocytes (data not shown). No such structures were observed in control, H_2O-injected oocytes (Figure 1f).

The serine lipase active site of MLN1 is required for its ability to generate tubulo-vesicular structures

Given the known cation channel activity of MLN1, we initially surmised that over-expression of this protein was causing a disturbance in the transmembrane gradients for Ca^{2+} and/or other cations, which caused osmotic stress and resulted in the formation of membrane blebs and vesicles. However, we did not observe the formation of similar structures in oocytes expressing other Ca^{2+}-permeable cation channels of the TRP family, e.g., TRPP2, TRPPL, TRPV5 and TRPV6, all of which have large Ca^{2+} conductances [31-32].

Since MLN1 contains a consensus sequence for a serine lipase active site in the large loop between the first and second transmembrane domains (Figure 2a), we considered the possibility that this site is functional and may play a role in the action of MLN1 on membrane reshaping. For this purpose, we constructed an MLN1 mutant containing a modified, presumably inactive (see below) serine lipase active site (SL-MLN1). Visual comparison of oocytes injected with the cRNAs for the mutant SL-MLN1 or WT-MLN1 under the same conditions showed that no TVS were formed in the oocytes expressing SL-MLN1 (Figure 2b). However, they were abundantly generated in the oocytes expressing WT-MLN1 (Figures 1c-e; and 2c-e). Fluorescent subcellular clusters containing the GFP-tagged SL-MLN1 are evident in the subcortical regions of oocytes expressing this mutant (Figure 2b). These clusters, however, do not lead to budding and extrusion of TVS as seen in the WT-MLN1-expressing oocytes. These data suggest that the serine lipase site of MLN1 is essential for formation of the TVS (Figure 2c-e). Examination of a twisted tubular formation that was extruded from an oocyte expressing GFP-tagged WT-MLN1 shows that MLN1 is predominantly located in the leading edge of the tubule (Figure 2d). Furthermore, there are several striations of GFP fluorescence in this area, with indentations on the sides of the tubular structure, perhaps illustrating the initial points at which vesicles are pinched off from the tubule. Figure 2e shows a larger area of a different oocyte where the GFP-tagged MLN1 is again mainly localized near the advancing edge of a large protrusion toward the upper right side of the field, and a non-specific red autofluorescence becomes apparent in the lower area on the opposite end of the oocyte. No such TVS are observed in oocytes expressing GFP-tagged SL-MLN1 (Figure 2f) or in H_2O-injected oocytes where only the red autofluorescence is evident (Figure 2g). Figure 2h shows that the percentage of oocytes producing TVS markedly increases after day 2 in both actinomycin D-treated (ML+ACT) and untreated oocytes expressing WT-MLN1 (ML) ($p < 0.05$ compared with the corresponding basal value), while no such structures were observed in H_2O-injected oocytes (H_2O) or in oocytes expressing the SL-MLN1 mutant (SL). We found similar levels of GFP fluorescence intensity after injection of oocytes with WT-MLN1-GFP or SL-MLN1-GFP

cRNAs (Figure 2i), indicating that the membrane reshaping effects that we observed were not merely due to higher expression of the WT-MLN1 versus the SL-MLN1 proteins in the respective batches of oocytes.

Mutation of the serine lipase active site abolishes the phospholipase activity

Since MLN1 is a membrane protein integrated into the phospholipid bilayer, we explored the possibility that it may act as a phospholipase (PL). Based on the evidence that the serine lipase site in MLN1 plays a role in membrane remodeling, we set out to define the type of lipase activity mediated by this protein. We utilized fluorescent probes for phospholipase A_1 and A_2 (PLA_1/A_2) and obtained evidence indicating that wild type MLN1 can mediate phospholipase A (PLA). After homogenizing the oocytes, we tested their PLA activities using the bis-BODIPY FL C_{11}-PC probe [20] for PLA_1/A_2, which was used to study the functional expression in *Xenopus laevis* oocytes of another recently cloned lysosomal PLA2 [21]. In this latter study on whole oocyte homogenates, an increase in PLA2 activity of more than 40% above the background level (H_2O-injected oocytes) was measured with this probe in oocytes expressing PLA2, similar to the values we observed on day four in oocytes expressing WT-MLN1 (Figure 3a). We also used a probe that is specific for PLA2, Bodipy FL C_5–HPC, and obtained similar results. The PLA activity in WT-MLN1-expressing oocytes increased considerably several days after injection of the oocytes with WT-MLN1 cRNA ($p < 0.05$ compared with the corresponding basal value), while no substantial change in the background enzymatic activity occurred in the H_2O-injected oocytes (Figure 3a). The PLA activity in SL-MLN1-expressing oocytes was not increased significantly above that in the H_2O-injected oocytes. Thus the increase in PLA activity of WT-MLN1 occurring several days after injection (Figure 3a) corresponds to, and even precedes, the accumulation of TVS (Figure 2h). These results, together with the lack of significant changes in the H_2O-injected oocytes and in those expressing mutant SL-MLN1, suggest that the PLA activity of MLN1 plays a key role in the formation of these structures.

Similar channel activities of WT-MLN1 and SL-MLN1

We considered the possibility that the formation of the TVS is mediated not directly by the PLA activity but by changes in the MLN1 channel activity when its PLA activity is modulated. Therefore, we studied the channel properties of mutant SL-MLN1 in vesicles prepared from lysosomal membranes after their reconstitution by incorporation into liposomal membrane systems. We did not observe substantial differences between the channel characteristics of the SL-mutant (Figure 3b-e) and WT-MLN1. The Ca^{2+} and other cation conductances of SL-MLN1 were not significantly different from those of the WT-MLN1 (Figure 3b). The probability of channel opening (nPo) of both SL-MLN1 and WT-MLN1 gradually increased in vesicles prepared on subsequent days after injection of the oocytes (Figure 3c-e), apparently due to enhanced levels of expression and higher channel densities in the membranes. The increase in nPo of SL-MLN1 was not significantly different from that of WT-MLN1 (Figure 3e). This increase in nPo does not correspond to the insignificant change in PLA activity of SL-MLN1 (Figure 3a) and, therefore, cannot explain the lack of formation of TVS in and around the SL-MLN1-expressing oocytes. Despite the lack of substantial differences between the conductances and other channel characteristics of WT- and SL-MLN1 we cannot exclude indirect effects via some binding partners dependent on Ca^{2+} and other cations on the MLIV-related phenotypes.

The MLN1-stimulated exocytotic trafficking of lysosomes depends on its serine lipase active site

The sequence of events leading to the morphological changes described above is likely to include the translocation of lysosomes toward the cell periphery, resulting in fusion with the cell membrane and release of the lysosomal contents during exocytosis. We have previously

shown lysosomal exocytosis to be impaired in human fibroblasts derived from MLIV patients [18], but to be rescued after transfection with WT-MLN1. To assess lysosomal exocytosis in oocytes, we measured the amount of N-acetyl-beta-D-glucosaminidase (NAG) released by treatment with ionomycin, which promotes the Ca^{2+} dependent fusion of lysosomes with the PM (Figure 3f). NAG is a water-soluble, lysosome-specific enzyme in the lysosomal lumen whose activity has previously been characterized in *Xenopus* oocytes [22]. The NAG assay has principally been used in mammalian cells as a useful test for lysosomal exocytosis, and it has been shown that it is a ubiquitous phenomenon that occurs not only in specialized secretory cells but also in many other types of cells [16-17]. We found that the release of this enzyme from WT-MLN1-expressing whole oocytes is significantly higher than that from H_2O-injected (control) and SL-MLN1-expressing oocytes (Figure 3f) ($p<0.05$ for WT vs. control and WT vs. SL), particularly following stimulation with the Ca^{2+} ionophore, ionomycin. There was no statistically significant difference between the NAG release from the SL-MLN1-expressing oocytes and that from the H_2O-injected oocytes. These findings suggest that WT-MLN1 promotes the exocytotic trafficking of lysosomes, especially at higher levels of cytosolic Ca^{2+} after the application of the Ca^{2+} ionophore, and that its role in this process depends to a great extent on its serine lipase site.

Inhibitors of PLA2 impede the MLN1-mediated formation of TVS

To further characterize the PLA activity of MLN1, we studied the effects of various types of phospholipase inhibitors. An inhibitor of the secreted form of PLA2, bromo-phenacyl bromide (BPB), and another PLA2 inhibitor, aristolochic acid (AA), significantly reduced the enzyme activity associated with the expression of MLN1, while inhibitors of phospholipase C (PLC) and phospholipase D (PLD) did not produce substantial reductions (Figure 3g).

To assess the contribution of the PLA activity to the generation of TVS, we tested the actions of the phospholipase inhibitors on this phenomenon. The formation of these structures was inhibited in WT-MLN1-expressing oocytes treated with the PLA2 inhibitors, BPB and AA. We assessed the gradual increase in the percentage of oocytes with associated TVS and found that BPB and AA inhibited the generation of these structures in WT-MLN1-expressing oocytes on day 8 by 48% and 56%, respectively, while the PLC and PLD inhibitors had no significant effect (Figure 3h). The time-course of the formation of these structures is similar to that of the increase in PLA activity of WT-MLN1 (Figure 3a), and their reduction by PLA2 inhibitors corresponds to the antagonistic effects of these inhibitors on the MLN1-associated PLA activity (Figure 3g).

Generation of TVS *in vitro* using a model membrane system is dependent on the serine lipase site of MLN1

To further explore the role of MLN1-associated PLA activity in membrane remodeling, we carried out studies using in vitro translated MLN1 fragments and a model membrane system. We expressed the soluble fragment spanning the lumenal loop of MLN1 that contains the serine lipase active site (See Figure 2a). The fragment was expressed as a fusion protein that contained a His-tag for purification and an X-press epitope for identification by Western blot (Figure 4a). We also expressed a corresponding SL-MLN1 fragment. We used thin layer chromatography (TLC) to characterize the PLA2 activity associated with MLN1. We measured the amounts of the fluorescent products formed during incubation with WT-MLN1 and SL-MLN1 protein extracts and confirmed that the WT-MLN1 extract with its intact serine lipase active site generated the expected products of PLA2 activity, while the SL-MLN1 fragment failed to elicit such an effect (Figure 4b). The PLA2-associated activity of WT-MLN1 was reduced significantly by the PLA2 inhibitors, BPB and AA (Figure 4b). The effects of the WT lipase fragment on various substrates were compared. No significant

differences were found for the following substrates: bis-Bodipy FL C_{11}-PC (0.814+/−0.07,+/−SEM, n=5), Bodipy FL C_5-HPC (0.906+/−0.082,+/−SEM, n=5), and PED6 (0.871+/−0.065,+/−SEM, n=5). Both bis-Bodipy FL C_{11}-PC and Bodipy FL C_5-HPC are phosphatidylcholines, but the chain length of the cleavable fluorescent fatty acid of Bodipy FL C_5-HPC is shorter than that of bis-Bodipy FL C_{11}-PC. PED6 is a different type of phospholipid, namely a phosphatidylethanolamine [20]. These results suggest that the PLA2 activity associated with MLN1 is similar for fatty acids of varying chain lengths, and for different types of phospholipids. The pH dependence of the enzymatic activity of MLN1 was weak. At pH 7.4, the activity was 0.688+/−0.075 (+/−SEM, n=5), only 21.8% lower than that at pH 5 (0.906+/−0.082, +/−SEM, n=5).

We were also able to reproduce the effects of WT-MLN1 on membrane reshaping generated *in vitro* using a model membrane system. We found that the *in vitro* translated lumenal loop fragment of WT-MLN1 mediated the formation of tubule-vesicular structures from liposome vesicles (Figure 4c), while the loop fragment of the SL mutant did not exert such an action (Figure 4d). In studies on liposomes containing different fluorescent probes and phospholipids, we found that the WT-MLN1 fragment mediated the formation of long and short tubules resembling cell extensions and multiple fusing vesicular structures (Figure 4e-j and l), while the SL-MLN1 fragment failed to generate such structures (Figure 4k and l). Both of the PLA2 inhibitors, BPB and AA, reduced significantly the formation of tubules as shown by our quantitative analysis (Figure 4l). The values for tubule formation after 2h and 4h incubation in the presence of the WT-MLN1 fragment were 21.8+/−3.12% (n=4), and 73.6+/−5.17% (n=4), respectively. They were normalized in relation to the value observed after 5h incubation (100%). The formation of tubules at pH 7.4 (81.24+/−5.69%, n=5) was only slightly lower (18.76%) than that at pH 5 (100%, value for normalization). The results obtained using the model membrane system suggest that the serine lipase active site on the loop fragment of MLN1 is associated with PLA2 activity and further, that this serine lipase domain is directly involved in membrane vesicular remodeling and potentially, in the growth of tubular structures.

MLN1 mediates TVS formation on the surface of human fibroblasts

The role of the serine lipase domain in mammalian cells should be explored. A patient has recently been identified with a point mutation in the serine lipase active site of the MCOLN1 gene, resulting in an amino acid substitution, 106/Leu→Pro (L106P) in the MLN1 protein [19]. Although we stop short of showing that the serine lipase domain on MLN1 directly mediates PLA2 activity, collectively these results demonstrate that the PLA2 activity associated with MLN1 plays a role in membrane reshaping. Our experiments were performed using semi-purified fusion proteins from *E. coli* and in vitro translated products formed in rabbit reticulocyte lysates. Both of these systems could potentially be contaminated with exogenous PLA2 enzymes. However we would expect that any such contaminating PLA2 activity would be equally represented in both the WT and SL preparations. In light of the possibility that the membrane reshaping that we observed in these artificial systems was the indirect result of the contamination by a nonspecific PLA2, we sought to determine whether MLN1 could be associated with similar phenomenon *in vivo*, in a mammalian cell.

We examined the cell surface topology of human primary dermal fibroblasts. We stained the surface of the fibroblasts with CMDiI and a variety of other fluorescent agents and viewed them at 400x magnification. We observed a number of enlarged bulb-shaped TVS protruding from the upper surface and from the ends of the processes of nearly every cell in the normal fibroblast population (Figure 5 a-g). When counterstained with lysosomal dyes we found that these TVS frequently contained LE/L organelles. Figure 5a shows a cluster of intracellular orgenelles stained with LysoTracker® Red DND-99, inside a process that is

also labeled with the green cytosolic dye, calcein. We used the same cytosolic probe in combination with another red fluorescent probe, Red DiI-C16(3), which preferentially stains membranes from the LE/L pathway [33] and observed a similar pronounced distribution of intracellular LE/L organelles along a cellular process and often near the plasma membrane (Figure 5b). The localization of LE/L organelles inside the extensions suggests the involvement of LE/L membrane components in their functions and reshaping. We explored the distribution of GFP-tagged MLN1 expressed in normal fibroblasts. Although the GFP-tagged WT-MLN1 is predominantly localized within the perinuclear region in the interior of the cell (not shown), we found that a substantial amount of MLN1 is located near the cell surfaces as well as in cellular processes (Figure 5c and d). We often observed bulb-shaped TVS (examples marked with arrow heads in Fig 5d and e) in normal fibroblasts, along the processes or at their tips (Figure 5d-f). Figure 5d shows that the MLN1 is also located in densely packed patches on the plasma membrane of the bulb-shaped TVS. These patches may represent the sites where the LE/L organelles have merged with the plasma membrane.

The lipophilic fluorescent probe, $DiIC_{16}(3)$ can be used as a lipophilic marker of the lumenal leaflet of the LE/L membrane because it is not prone to flip-flop from the lumenal to the cytosolic leaflet of the bilayer [33]. We found that after internalization and intracellular trafficking, a small percentage of the probe is translocated out to the plasma membrane of normal fibroblasts within a few hours, with a concentration in the surface membrane of the filapodia and filapodia-like processes and bulb-shaped TVS (Figure 5f and h). Fluorescent staining can also be found on the surface of nanotubular processes that resemble cytonemes and tunneling nanotubes (TNTs), which are actin-filled membrane processes of approximately 200 nm in diameter but often tens of microns in length [28,34-36].

In Figure 5e, where the cells are co-stained with the red probe, $DiIC_{16}(3)$, and the green cytosolic probe calcein, three enlarged bulb-shaped TVS are observed along a TNT. Red and yellow stained LE/L vesicles are found inside these vesicles, as well as in the interior of the cellular processes, but there is also substantial staining on the cell surface continuous with the plasma membrane of the nanotubular processes that connect the vesicles (Figure 5e, f and h). In MLIV cells that express no MLN1 we observed intense intracellular LE/L vesicle staining with this probe, but the plasma membrane was only weakly stained, perhaps due to the deficient trafficking and lysosomal exocytosis in the MLIV cells (Figures 5g and i). The intensity of the plasma membrane staining in normal and MLIV cells can be compared between figures 5h and 5i, in which the edges of the respective plasma membranes are indicated by open arrows (note the deficiency in PM staining at the edge marked by open arrow on Figure 5i). In order to quantify the vesicles in each population, we visualized the vesicles under confocal microscopy. Figure 5f, and the enlarged inset shown in 5h, show the typical cross-sections of bulb-shaped vesicle as they appear in single confocal planes (red arrows). Although such vesicles can be observed in MLIV cells (red arrows in Figure 5i), they tend to be smaller, fewer in number, with lower intensity $DiIC_{16}(3)$ staining (Figure 5g and 5i, green arrows in 5i). We used digital image analysis to measure the percentage of total cellular area per field that was occupied by cell surface vesicles (Percent TVS Area). We found that the percentage occupied by vesicles was 64% lower in MLIV fibroblasts than in normal fibroblasts When normalized, the TVS Ratio was 2.77 +/−0.34 fold higher in normal cells, relative to MLIV cells ($p < 0.01$ **; n=14)(Figure 5j).

Expression of GPF-tagged MLN1 cDNA constructs in MLIV fibroblasts

To confirm an association between MLN1 and the bulb-shaped TVS on fibroblasts, we transfected MLIV cells with GFP-tagged WT-MLN1 cDNA, or with cDNA constructs with point mutations in the serine lipase (SL and L106P mutants) or ion channel domains (F465L mutant). We verified expression and correct localization of the GFP-tagged fusion protein to

the lysosomes. In all constructs, the expressed GFP-tagged protein co-localized with the acidic LysoTracker Red-stained vesicles to a similar extent (Table 1). This finding is consistent with the lysosomal localization of MLN1 as shown in other studies [37-38]. We were also able to detect translocation of the lysosomes out to the bulb-shaped TVS in WT and mutant cDNA transfections, suggesting that intracellular vesicle trafficking was not affected in the respective mutations (not shown).

We measured the Percent TVS Area in the transfected MLIV cells. We documented the restoration of bulb-shaped TVS on the cell surface of WT-transfected MLIV fibroblasts to levels approaching that of normal untransfected fibroblasts, whereas transfection with pcDNA vector did not significantly alter the level of TVS relative to untransfected MLIV cells. When the data was normalized to the vector-transfected MLIV control, the TVS Ratio of WT-transfected fibroblasts was 2.46 +/−0.37 ($p < 0.01$ **; n=12), approaching the ratio of 2.77 +/− 0.34 that we found in untransfected fibroblasts (Figure 5j).

Some of the events associated with lysosomal trafficking, including fusion of the lysosomes with the plasma membrane, could potentially be mediated by the opening of the MLN1 channel or the phospholipase activity, or both. The role of the channel in the mechanism of formation of TVS, and its relationship to the serine lipase activity, is not yet understood. For this reason we examined the contribution of the individual domains by expressing MLN1 cDNAs with point mutations that affected either the lipase or channel activity. We expressed two separate cDNAs with lipase point mutants, SL the engineered lipase knockout, and L106P, a naturally occurring point mutation found in an MLIV patient [19]. We compared the plasma membrane surface topology in the cells transfected with the SL mutant constructs to those transfected with the WT-MLN1 construct or the empty vector. In contrast to the WT-MLN1 construct, neither the SL nor the L106P mutants was able to significantly restore TVS formation on the cell surface above the level of vector transfected MLIV cells, with TVS Ratios of 1.23 +/−0.18 (p=0.28, n=9), and 0.93 +/−0.18 (p=0.73, n=9), respectively (Figure 5j), despite the presence of a functional channel domain in these constructs (Figure 3b-e). We also transfected the MLIV cells with a cDNA expressing the 465/Phe→Leu mutation (F465L) that inactivates channel function [39] but contains a normal serine lipase site. It is interesting to note that the F465L-transfected cells showed a significant, albeit limited, restoration of TVS formation (TVS Ratio = 1.68 +/−0.25, ($p < 0.05$ *, n=9)), despite the absence of a functional channel (Figure 5j). These data suggest that both the channel and the serine lipase motif may play separate roles in the formation of TVS, but the serine lipase domain appears to predominate in this aspect of membrane remodeling. The roles of MLN1's channel and serine lipase domains, as well as the potential contributions of accessory proteins such as TRPML2 and TRPML3 and other endogenous channels may play a partial compensatory role in some of the phases of these processes in MLIV cells, and will need to be examined in separate studies.

Role of MLN1-associated PLA2 activity in membrane remodeling

We have obtained evidence that MLN1 can mediate phospholipase activity by virtue of its serine lipase active site on the large lumenal loop between the first and second transmembrane domains. The results obtained using the three different systems, oocytes, model membrane vesicles and human fibroblasts, corroborate one another, suggesting that the serine lipase active site of MLN1 is required for its effects on membrane remodeling. The TVS in oocytes are larger than those in the model membrane system but most of the TVS are proportionate in size relative to the structures from which they were formed (e.g., oocytes and model membrane vesicles). Further study will be needed to determine whether MLN1 conveys the enzymatic activity directly, or merely facilitates the activity of an associated phospholipase.

The mechanism by which MLN1 influences membrane reshaping remains to be determined. Several potential mechanisms may be considered. Prior studies have demonstrated that direct application of different types of phospholipases, including PLA2, to large liposomes mediated vesicle budding and further remodeling of liposomal membranes [40-42]. The effects observed in model membrane systems cannot be explained by activation of signaling pathways and are apparently mediated by direct spontaneous reshaping of the phospholipid bilayers by the phospholipases [43]. The lysophospholipids produced as cleavage products of PLA2 have inverted conical shapes that promote convex outward orientation of membrane bending, conventionally referred to as positive curvature, on the adjacent leaflet of the bilayer. This has been proposed to influence, in turn, a negative curvature of the other face [44-46] (Figure 6a and b).

Role of PLA2-mediated membrane remodeling in the formation of TVS

Considering the localization of MLN1's lipase domain on the lumenal face of LE/L, it is conceivable that it may act during several potential steps leading to the formation of TVS on the cell surface. We have previously shown that overexpression of MLN1 is associated with enhanced lysosomal exocytosis in human fibroblasts and in Xenopus oocytes coinciding with increased MLN1 channel activity on the plasma membrane, suggesting that MLN1 is translocated to the surface within these patches [1,18]. The phospholipase activity associated with the luminal leaflet which would be found on the outer surface of the plasma membrane after exocytosis, is likely to promote the outward curvature. The domain may enable the curvature on the lumenal leaflet at the neck of the fusion junction between the lysosome and the plasma membrane during exocytosis (Fig 6c) [42,44,47]. The accumulation of conical lysophospholipids, perhaps in conjunction with the coordinated actions of accessory proteins in physiological systems that promote membrane curvature such as cytoskeletal and scaffold proteins and lysophosphatidic acid acyl transferase (LPAT), may also be involved as the lumenal face is inverted to the extracellular face (6c-e). In addition, the phospholipase may act on the cell surface to modify lipids on the plasma membrane and incorporate them into the growing TVS [48]. The percentage of inverted cone-shaped lipids in outer vs. inner leaflets could influence the diameter of tubular extensions as well [46] (Figure 6b). Although the actual role of MLN1 in the formation of TVS remains to be determined, the phospholipase activity associated with the protein may facilitate one or more of these steps in membrane trafficking.

In addition to the membrane reshaping steps proposed above, MLN1 may also be involved in facilitating bilayer fusion as the LE/L membranes are integrated into the plasma membrane. Several recent reports have implicated phospholipases in bilayer fusion both *in vitro* and *in vivo* [49-56]. A number of biophysical studies have been undertaken in recent years to sort out the mechanism by which the phospholipases affect membrane fusion, but it has been suggested that in addition to creating conical lipids that deform the bilayer, lipids may also act by increasing the fluidity within a localized region of the bilayer or generating a defect that creates a local instability in the membrane. The phospholipase activity associated with the integral membrane protein, MLN1, within the double bilayer fusion zone could be directly involved in localized enzymatic degradation of the phospholipids. Thus it could help to overcome the barrier of the double hydrophobic bilayer by creating the local membrane disruption or remodeling needed to initiate the formation of the fusion pore. Local disruptions in either leaflet of the plasma membrane may also serve as initial sites where the growing cytoskeletal structures may mediate or contribute to the formation of membrane protrusions and outgrowth of cellular extensions.

In conclusion, this study shows that MLN1, a channel protein of the TRP family, can mediate phospholipase activity that contributes to the formation of membrane vesicular and tubular structures via its serine lipase active site. Thus MLN1 represents a novel type of

bifunctional protein that plays a role in cell surface restructuring and potentially in the formation of cell processes.

Acknowledgments

The authors wish to kindly thank Dr. James Gusella for his helpful discussions during the preparation of this manuscript. This study was supported by the ML4 Foundation (JML), the National Institute of Neurological Disorders and Stroke NS39995 (SAS), NIH, PKDF, Genzyme, NARSAD and Stanley Foundation (PMV).

REFERENCES

[1]. LaPlante JM, Falardeau J, Sun M, Kanazirska M, Brown EM, Slaugenhaupt SA, Vassilev PM. Identification and characterization of the single channel function of human mucolipin-1 implicated in mucolipidosis type IV, a disorder affecting the lysosomal pathway. FEBS Lett. 2002; 532:183–187. [PubMed: 12459486]

[2]. Raychowdhury MK, Gonzalez-Perrett S, Montalbetti N, Timpanaro GA, Chasan B, Goldmann WH, Stahl S, Cooney A, Goldin E, Cantiello HF. Molecular pathophysiology of mucolipidosis type IV: pH dysregulation of the mucolipin-1 cation channel. Hum Mol Genet. 2004; 13:617–627. [PubMed: 14749347]

[3]. LaPlante JM, Ye CP, Quinn SJ, Goldin E, Brown EM, Slaugenhaupt SA, Vassilev PM. Functional links between mucolipin-1 and Ca2+-dependent membrane trafficking in mucolipidosis IV. Biochem Biophys Res Commun. 2004; 322:1384–1391. [PubMed: 15336987]

[4]. Bargal R, Avidan N, Ben-Asher E, Olender Z, Zeigler M, Frumkin A, Raas-Rothschild A, Glusman G, Lancet D, Bach G. Identification of the gene causing mucolipidosis type IV. Nat Genet. 2000; 26:118–123. [PubMed: 10973263]

[5]. Bassi MT, Manzoni M, Monti E, Pizzo MT, Ballabio A, Borsani G. Cloning of the gene encoding a novel integral membrane protein, mucolipidin-and identification of the two major founder mutations causing mucolipidosis type IV. Am J Hum Genet. 2000; 67:1110–1120. [PubMed: 11013137]

[6]. Sun M, Goldin E, Stahl S, Falardeau JL, Kennedy JC, Acierno JS Jr. Bove C, Kaneski CR, Nagle J, Bromley MC, Colman M, Schiffmann R, Slaugenhaupt SA. Mucolipidosis type IV is caused by mutations in a gene encoding a novel transient receptor potential channel. Hum Mol Genet. 2000; 9:2471–2478. [PubMed: 11030752]

[7]. Berman ER, Livni N, Shapira E, Merin S, Levij IS. Congenital corneal clouding with abnormal systemic storage bodies: a new variant of mucolipidosis. J Pediatr. 1974; 84:519–526. [PubMed: 4365943]

[8]. Bach G, Cohen MM, Kohn G. Abnormal ganglioside accumulation in cultured fibroblasts from patients with mucolipidosis IV. Biochem Biophys Res Commun. 1975; 66:1483–1490. [PubMed: 1191304]

[9]. Bach G, Desnick RJ. Lysosomal accumulation of phospholipids in mucolipidosis IV cultured fibroblasts. Enzyme. 1988; 40:40–44. [PubMed: 3168971]

[10]. Bach G, Ziegler M, Kohn G, Cohen MM. Mucopolysaccharide accumulation in cultured skin fibroblasts derived from patients with mucolipidosis IV. Am J Hum Genet. 1977; 29:610–618. [PubMed: 145180]

[11]. Bargal R, Bach G. Phospholipids accumulation in mucolipidosis IV cultured fibroblasts. J Inherit Metab Dis. 1988; 11:144–150. [PubMed: 3139925]

[12]. Fares H, Greenwald I. Regulation of endocytosis by CUP-5, the Caenorhabditis elegans mucolipin-1 homolog. Nat Genet. 2001; 28:64–68. [PubMed: 11326278]

[13]. Bargal R, Bach G. Mucolipidosis type IV: abnormal transport of lipids to lysosomes. J Inherit Metab Dis. 1997; 20:625–632. [PubMed: 9323557]

[14]. Soyombo AA, Tjon-Kon-Sang S, Rbaibi Y, Bashllari E, Bisceglia J, Muallem S, Kiselyov K. TRP-ML1 regulates lysosomal pH and acidic lysosomal lipid hydrolytic activity. J Biol Chem. 2006; 281:7294–7301. [PubMed: 16361256]

[15]. Gerasimenko JV, Gerasimenko OV, Petersen OH. Membrane repair: Ca(2+)-elicited lysosomal exocytosis. Curr Biol. 2001; 11:R971–974. [PubMed: 11728325]

[16]. Reddy A, Caler EV, Andrews NW. Plasma membrane repair is mediated by Ca(2+)-regulated exocytosis of lysosomes. Cell. 2001; 106:157–169. [PubMed: 11511344]

[17]. Rodriguez A, Webster P, Ortego J, Andrews NW. Lysosomes behave as Ca2+-regulated exocytic vesicles in fibroblasts and epithelial cells. J Cell Biol. 1997; 137:93–104. [PubMed: 9105039]

[18]. LaPlante JM, Sun M, Falardeau J, Dai D, Brown EM, Slaugenhaupt SA, Vassilev PM. Lysosomal exocytosis is impaired in mucolipidosis type IV. Mol Genet Metab. 2006; 89:339–348. [PubMed: 16914343]

[19]. Altarescu G, Sun M, Moore DF, Smith JA, Wiggs EA, Solomon BI, Patronas NJ, Frei KP, Gupta S, Kaneski CR, Quarrell OW, Slaugenhaupt SA, Goldin E, Schiffmann R. The neurogenetics of mucolipidosis type IV. Neurology. 2002; 59:306–313. [PubMed: 12182165]

[20]. Farber SA, Pack M, Ho SY, Johnson ID, Wagner DS, Dosch R, Mullins MC, Hendrickson HS, Hendrickson EK, Halpern ME. Genetic analysis of digestive physiology using fluorescent phospholipid reporters. Science. 2001; 292:1385–1388. [PubMed: 11359013]

[21]. Kim TS, Sundaresh CS, Feinstein SI, Dodia C, Skach WR, Jain MK, Nagase T, Seki N, Ishikawa K, Nomura N, Fisher AB. Identification of a human cDNA clone for lysosomal type Ca2+-independent phospholipase A2 and properties of the expressed protein. J Biol Chem. 1997; 272:2542–2550. [PubMed: 8999971]

[22]. Prody GA, Greve LC, Hedrick JL. Purification and characterization of an N-acetyl-beta-D-glucosaminidase from cortical granules of Xenopus laevis eggs. J Exp Zool. 1985; 235:335–340. [PubMed: 4056694]

[23]. Dargan SL, Lea EJ, Dawson AP. Modulation of type-1 Ins(1,4,5)P3 receptor channels by the FK506-binding protein, FKBP12. Biochem J. 2002; 361:401–407. [PubMed: 11772413]

[24]. Vassilev PM, Kanazirska MP, Tien HT. Ca2+ channels from brain microsomal membranes reconstituted in patch-clamped bilayers. Biochim Biophys Acta. 1987; 897:324–330. [PubMed: 2434130]

[25]. Vassilev PM, Tien HT. Reconstitution of membrane molecular mechanisms in bilayer lipid membranes and patch-clamp bilayers. Subcell Biochem. 1989; 14:97–143. [PubMed: 2655201]

[26]. Carpenter AE, Jones TR, Lamprecht MR, Clarke C, Kang IH, Friman O, Guertin DA, Chang JH, Lindquist RA, Moffat J, Golland P, Sabatini DM. CellProfiler: image analysis software for identifying and quantifying cell phenotypes. Genome Biol. 2006; 7:R100. [PubMed: 17076895]

[27]. Lamprecht MR, Sabatini DM, Carpenter AE. CellProfiler: free, versatile software for automated biological image analysis. Biotechniques. 2007; 42:71–75. [PubMed: 17269487]

[28]. Ramirez-Weber FA, Kornberg TB. Cytonemes: cellular processes that project to the principal signaling center in Drosophila imaginal discs. Cell. 1999; 97:599–607. [PubMed: 10367889]

[29]. Gould SJ, Booth AM, Hildreth JE. The Trojan exosome hypothesis. Proc Natl Acad Sci U S A. 2003; 100:10592–10597. [PubMed: 12947040]

[30]. Galkina SI, Sud'ina GF, Ullrich V. Inhibition of neutrophil spreading during adhesion to fibronectin reveals formation of long tubulovesicular cell extensions (cytonemes). Exp Cell Res. 2001; 266:222–228. [PubMed: 11399050]

[31]. Vassilev PM, Peng JB, Hediger MA, Brown EM. Single-channel activities of the human epithelial Ca2+ transport proteins CaT1 and CaT2. J Membr Biol. 2001; 184:113–120. [PubMed: 11719848]

[32]. Chen XZ, Vassilev PM, Basora N, Peng JB, Nomura H, Segal Y, Brown EM, Reeders ST, Hediger MA, Zhou J. Polycystin-L is a calcium-regulated cation channel permeable to calcium ions. Nature. 1999; 401:383–386. [PubMed: 10517637]

[33]. Mukherjee S, Soe TT, Maxfield FR. Endocytic sorting of lipid analogues differing solely in the chemistry of their hydrophobic tails. J Cell Biol. 1999; 144:1271–1284. [PubMed: 10087269]

[34]. Onfelt B, Davis DM. Can membrane nanotubes facilitate communication between immune cells? Biochem Soc Trans. 2004; 32:676–678. [PubMed: 15493985]

[35]. Gerdes HH, Bukoreshtliev NV, Barroso JF. Tunneling nanotubes: a new route for the exchange of components between animal cells. FEBS Lett. 2007; 581:2194–2201. [PubMed: 17433307]

[36]. Rustom A, Saffrich R, Markovic I, Walther P, Gerdes HH. Nanotubular highways for intercellular organelle transport. Science. 2004; 303:1007–1010. [PubMed: 14963329]

[37]. Manzoni M, Monti E, Bresciani R, Bozzato A, Barlati S, Bassi MT, Borsani G. Overexpression of wild-type and mutant mucolipin proteins in mammalian cells: effects on the late endocytic compartment organization. FEBS Lett. 2004; 567:219–224. [PubMed: 15178326]

[38]. R F, Pryor PR, Gribble FM, Luzio JP. Mucolipin-1 is a lysosomal membrane protein required for intracellular lactosylceramide traffic. Traffic. 2006; 7:1388–1398. [PubMed: 16978393]

[39]. Kiselyov K, Chen J, Rbaibi Y, Oberdick D, Tjon-Kon-Sang S, Shcheynikov N, Muallem S, Soyombo A. TRP-ML1 is a lysosomal monovalent cation channel that undergoes proteolytic cleavage. J Biol Chem. 2005; 280:43218–43223. [PubMed: 16257972]

[40]. Holopainen JM, Angelova MI, Soderlund T, Kinnunen PK. Macroscopic consequences of the action of phospholipase C on giant unilamellar liposomes. Biophys J. 2002; 83:932–943. [PubMed: 12124275]

[41]. Holopainen JM, Angelova MI, Kinnunen PK. Vectorial budding of vesicles by asymmetrical enzymatic formation of ceramide in giant liposomes. Biophys J. 2000; 78:830–838. [PubMed: 10653795]

[42]. Staneva G, Angelova MI, Koumanov K. Phospholipase A2 promotes raft budding and fission from giant liposomes. Chem Phys Lipids. 2004; 129:53–62. [PubMed: 14998727]

[43]. Kooijman EE, Chupin V, Fuller NL, Kozlov MM, de Kruijff B, Burger KN, Rand PR. Spontaneous curvature of phosphatidic acid and lysophosphatidic acid. Biochemistry. 2005; 44:2097–2102. [PubMed: 15697235]

[44]. Brown WJ, Chambers K, Doody A. Phospholipase A2 (PLA2) enzymes in membrane trafficking: mediators of membrane shape and function. Traffic. 2003; 4:214–221. [PubMed: 12694560]

[45]. Huttner WB, Schmidt AA. Membrane curvature: a case of endofeelin'. Trends Cell Biol. 2002; 12:155–158. [PubMed: 11978528]

[46]. Sheetz MP, Singer SJ. Biological membranes as bilayer couples. A molecular mechanism of drug-erythrocyte interactions. Proc Natl Acad Sci U S A. 1974; 71:4457–4461. [PubMed: 4530994]

[47]. Schmidt A, Wolde M, Thiele C, Fest W, Kratzin H, Podtelejnikov AV, Witke W, Huttner WB, Soling HD. Endophilin I mediates synaptic vesicle formation by transfer of arachidonate to lysophosphatidic acid. Nature. 1999; 401:133–141. [PubMed: 10490020]

[48]. McMahon HT, Gallop JL. Membrane curvature and mechanisms of dynamic cell membrane remodelling. Nature. 2005; 438:590–596. [PubMed: 16319878]

[49]. Blackwood RA, Transue AT, Harsh DM, Brower RC, Zacharek SJ, Smolen JE, Hessler RJ. PLA2 promotes fusion between PMN-specific granules and complex liposomes. J Leukoc Biol. 1996; 59:663–670. [PubMed: 8656051]

[50]. Nagao T, Kubo T, Fujimoto R, Nishio H, Takeuchi T, Hata F. Ca(2+)-independent fusion of secretory granules with phospholipase A2-treated plasma membranes in vitro. Biochem J. 1995; 307(Pt 2):563–569. [PubMed: 7537492]

[51]. Nishio H, Takeuchi T, Hata F, Yagasaki O. Ca(2+)-independent fusion of synaptic vesicles with phospholipase A2-treated presynaptic membranes in vitro. Biochem J. 1996; 318(Pt 3):981–987. [PubMed: 8836147]

[52]. Cohen JS, Brown HA. Phospholipases stimulate secretion in RBL mast cells. Biochemistry. 2001; 40:6589–6597. [PubMed: 11380253]

[53]. Mayorga LS, Beron W, Sarrouf MN, Colombo MI, Creutz C, Stahl PD. Calcium-dependent fusion among endosomes. J Biol Chem. 1994; 269:30927–30934. [PubMed: 7983026]

[54]. Barbieri MA, Li G, Mayorga LS, Stahl PD. Characterization of Rab5:Q79L-stimulated endosome fusion. Arch Biochem Biophys. 1996; 326:64–72. [PubMed: 8579373]

[55]. Mayorga LS, Colombo MI, Lennartz M, Brown EJ, Rahman KH, Weiss R, Lennon PJ, Stahl PD. Inhibition of endosome fusion by phospholipase A2 (PLA2) inhibitors points to a role for PLA2 in endocytosis. Proc Natl Acad Sci U S A. 1993; 90:10255–10259. [PubMed: 8234286]

[56]. de Figueiredo P, Drecktrah D, Katzenellenbogen JA, Strang M, Brown WJ. Evidence that phospholipase A2 activity is required for Golgi complex and trans Golgi network membrane tubulation. Proc Natl Acad Sci U S A. 1998; 95:8642–8647. [PubMed: 9671731]

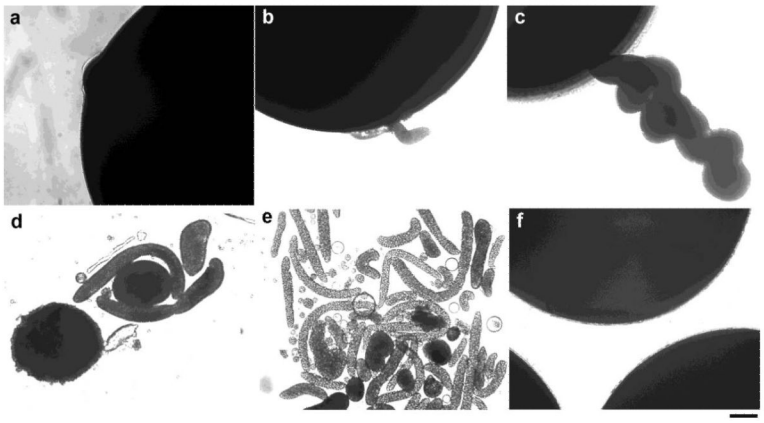

Figure 1. Tubulo-vesicular structures extruded from oocytes overexpressing wild type (WT) MLN1

Formation of these structures at 2-4 days after injection of WT-MLN1 cRNA (a and b), and at later stages 5-8 days after injection (c-e), are shown. No such structures were observed in control oocytes (injected with H_2O) (f) incubated for the same periods of time (1-8 days after injection). Scale bar: 100 μm.

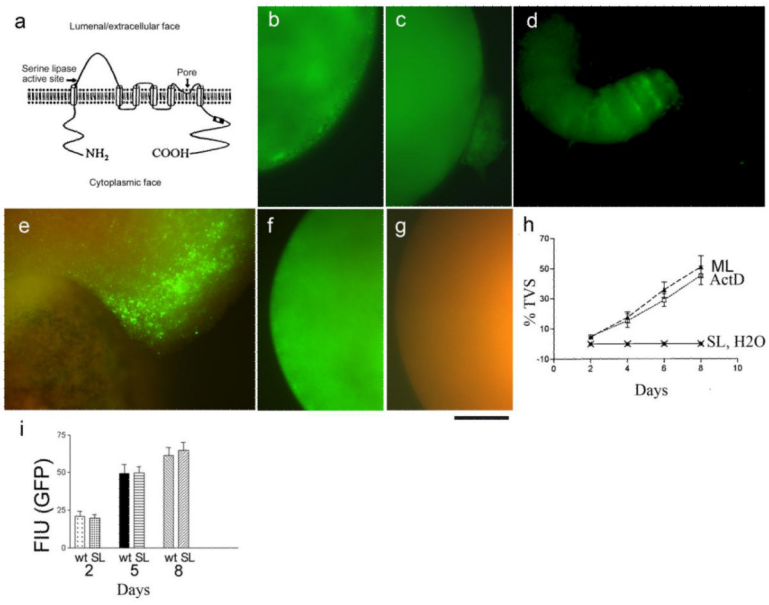

Figure 2. Formation of TVS is deficient in oocytes expressing MLN1 with a mutated serine lipase active site (SL-MLN1)

This site is located on the lumenal/extracellular side of MLN1 near its putative 1st transmembrane domain, while the pore region is between the putative 5th and 6th transmembrane domains (a). The oocyte shown in (b) has been injected with GFP-tagged SL-MLN1 mutant cRNA. Oocytes injected with GFP-tagged WT-MLN1 cRNA are shown in (c) and (d). Only the green fluorescence of the GFP-tagged proteins is shown in (b-d). Both GFP-emitted green fluorescence and nonspecific red autofluorescence from the oocyte contents are displayed in (e-g). (e) oocyte expressing GFP-tagged WT-MLN1), (f) oocyte expressing GFP-tagged SL-MLN1 mutant, and H_2O-injected oocyte (g). Scale bar: 100 μm. (h) Percentage of oocytes extruding TVS during the period of 1-8 days after injection of WT-MLN1 cRNA in untreated (ML) or actinomycin D-treated oocytes (ML+ACT), or after injection of SL-MLN1 cRNA (SL) or of H_2O (H_2O, coinciding with the symbols for SL) (+/− SEM, n=6). Single oocytes from the different groups were distributed in separate wells of 96-well plates, and all the wells were checked every day under the microscope to estimate the extrusion of TVS from the oocytes. In these experiments 25-80 oocytes were injected for each of these conditions. (i) Rates of increase in GFP fluorescence intensity after injection of oocytes with WT-MLN1 (wt) or SL-MLN1 cRNAs (SL), 2, 5 or 8 days after injection (+/−SEM, n=16).

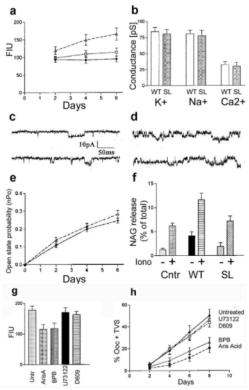

Figure 3. Comparison between the enzyme and channel activities and the contribution to lysosomal exocytosis of WT-MLN1 and SL-MLN1 mutant

In (a) the Bodipy FL C_{11}-PC probe was used to assess the phospholipase activities of WT-MLN1 (closed triangles), SL-MLN1 (open squares), and the control (H_2O-injected oocytes) (+/−SEM, n=12). The activity was estimated in LE/L-containing oocyte extracts for each of these groups by measuring the increase in fluorescence intensity units (FIU) several days after injection. In (b) the K+, Na+, and Ca2+ conductances, expressed in picosiemens (pS), of WT-MLN1 (open bars) and SL-MLN1 (dark bars) are compared. The unitary conductances were 81+/−6.4 pS (+/−SEM, n=8) for K+, 77.9+/−7.8 pS (n=8) for Na+, and 30.4+/−5.5 pS (n=8). Single channel traces were taken on day 2 (c) and day 6 (d) after injection of oocytes with WT-MLN1 cRNA (top traces) or SL-MLN1 cRNA (bottom traces). The traces were taken at −90 mV in the presence of 100 mM KCl in the pipette solution. The increase in open state probability (nPo) several days after injection (e) is similar in WT-MLN1-(open triangles) and SL-MLN1-expressing oocytes (closed circles) (+/−SEM, n=12). The lysosomal exocytosis was assessed by determining the amount of N-acetyl-beta-D-glucosaminidase (NAG) (+/−SEM, n=6) released into the bath solution from untreated whole oocytes (−) and from oocytes treated for 30 min with 10 μM ionomycin (+), as shown in (f). The three pairs of bars are marked underneath from left to right for H_2O-injected oocytes (Ctrl), or oocytes expressing either WT-MLN1 (WT) or SL-MLN1 (SL). The released amount of NAG is expressed as % of its total content in the cells, as explained in Methods. (g-h). Effects of phospholipase inhibitors on the enzyme activity and on the extrusion of TVS from oocytes expressing WT-MLN1. Panel (g) shows the changes in PLA activity of WT-MLN1 in LE/L-containing oocyte extracts (estimated by measuring the fluorescence of the Bodipy FL C_{11}-PC probe) mediated by the PLA_2 inhibitors, aristolochic acid (Aris, 40 μM) and bromophenacyl bromide (BPB, 40 μM), as well as by the inhibitor of phosphatidylinositol-specific PLC, U73122 (2 μM), and the inhibitor of phosphatidylcholine-specific PLC and PLD, D609 (40 μM) (+/−SEM, n=10). Panel (h) shows that BPB (open triangles) and ArisA (closed squares) markedly reduce the percentage of whole oocytes extruding TVS, while the inhibitors of PLC and PLD (crosses and open circles) do not show significant changes in comparison to the untreated oocytes (Untr.) (closed circles)(+/−SEM, n=6).

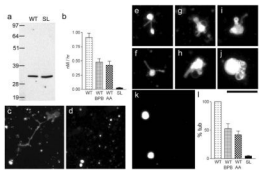

Figure 4. Phospholipase activity of MLN1 and evidence showing that the serine lipase site of MLN1 is required for the MLN1-mediated tubule formation from model membrane vesicles

Panel (a) shows Western blots of the WT and SL fragments of MLN1 produced *in vitro* as described in Methods. TLC and the Bodipy FL C_5 –HPC probe were used to measure the PLA_2 activity of the WT and SL fragments of MLN1 and the reduction of this activity of WT-MLN1 by 40 μM BPB and aristolochic acid (AA), as shown in (b). In the experiments on the model membrane system the WT-MLN1 fragment mediated formation of tubulo-vesicular structures after treating liposomes that were prepared from Folch fraction I phospholipids stained with sulforhodamine-PE for 5 hr at 37°C (c), while no such structures were observed with the SL-MLN1 fragment (d). The WT-MLN1 fragment also generated tubules and vesicular enlargements from liposomes formed from asolectin phospholipids stained with NBD-PS (e-j). The SL-MLN1 fragment again failed to produce such structures in this model membrane system (k). Panel (l) summarizes the quantitative data from the experiments on the liposomes. The percentage of tubular structures per field generated under each of the different conditions was normalized in relation to that mediated by the WT-MLN1 fragment that was taken as 100%. The PLA_2 inhibitors, BPB and aristolochic acid (AA), reduced significantly the number of tubular structures (+/−SEM, n=6). Scale bars are 50 μm.

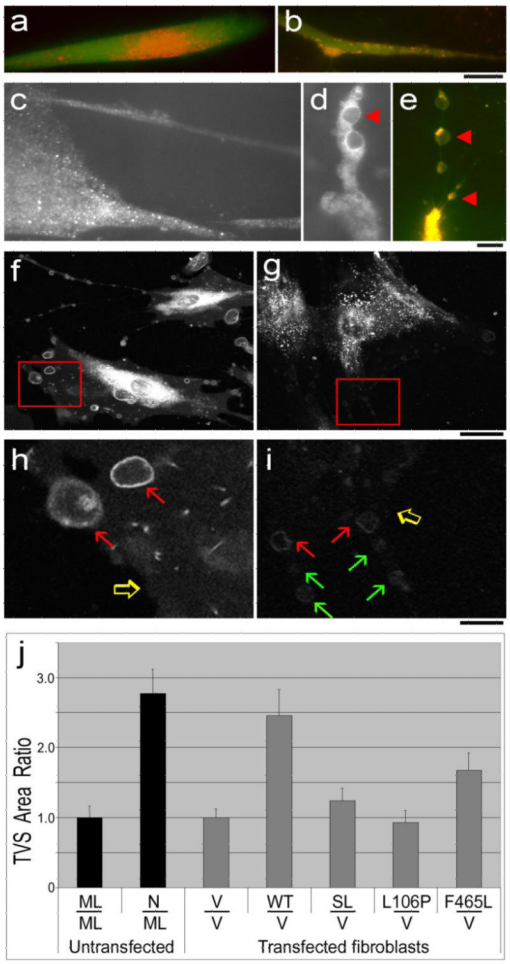

Figure 5. TVS on the surface of human fibroblasts

Fibroblasts from normal subjects co-stained with the green fluorescent probe, calcein (1uM), for visualizing the cytoplasm, and with calcein in combination with LysoTracker red DND99 in (a), calcein with the LE/L membrane probe, $DiIC_{16}(3)$ in (b and e), or $DiIC_{16}(3)$ without calcein (f-i). (Panels c and d), GFP fluorescence of normal fibroblasts transfected with GFP-tagged WT-MLN1, showing the localization of MLN1 on the cell surfaces, particularly in long thin processes (c) and on the perimeter of bulb-shaped TVS located along a process (d). Panel (e) depicts LE/L membrane staining along the perimeter of a series of bulb-shaped TVS connected by nanotubular tethers. For panels (a-e), scale bars are 10 um. In panels (d and e) representative bulb-shaped TVS are marked with arrowheads. Panels (f-i) show the surface of normal (f and h) or MLIV (g and i) fibroblasts. For panels (f-g) the scale bars correspond to 10 um. Panels (h) and (i) represent an enlarged view of the insets in panels (f) and (g), respectively. Scale bars correspond to 2.5 um. Panel (j) shows the results of the quantitative digital image analysis (CellProfiler). The percentage of total cellular area per 2 dimensional field that is occupied by the bulb-shaped TVS was calculated. Results were normalized to show the TVS Ratio of fibroblasts from normal subjects when normalized to MLIV fibroblasts (untransfected), or compares MLIV fibroblasts transfected with cDNA constructs containing the transcripts: WT, SL, L106P and F465L, when normalized to the vector-transfected MLIV fibroblasts.

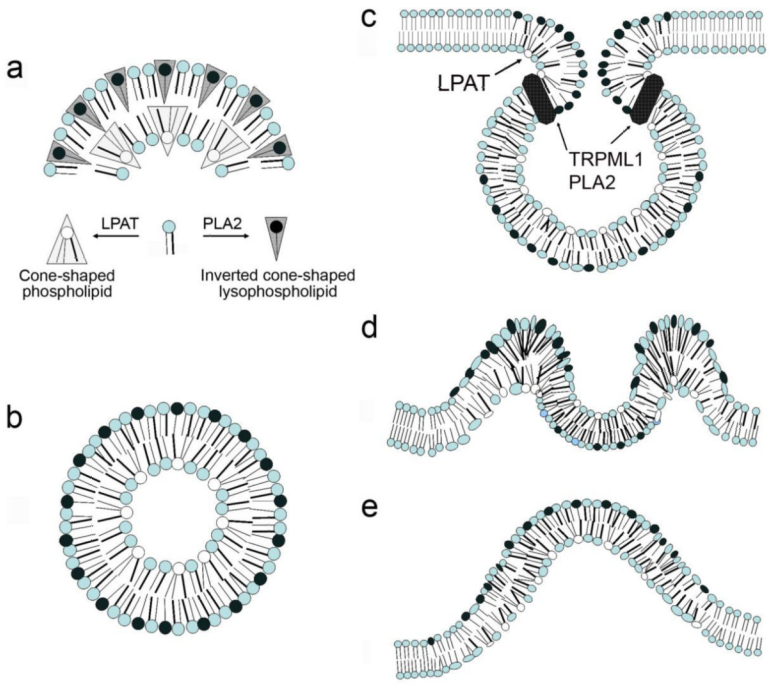

Figure 6. Potential topological changes related to the roles of MLN1-associated PLA2 activity in membrane remodeling

Panels (a-b), model depicting how introduction of conical shaped membrane phospholipids by PLA2s, or inverse conical shaped phospholipids by lysophosphatidic acid acyl transferase can lead to a biomechanical change in the shape of a lipid bilayer sheet (adapted from [44]). Panel (a), sagittal section of an outward membrane curvature, (b), cross-section of a tubular membrane process showing the role of membrane curvature in mediating the shape of a tubule. Panels (c-e), Proposed model for how the PLA2 could facilitate membrane remodeling during the extraversion of the lysosome and incorporation of its membrane into the TVS forming on the cell surface. (c) At the lumenal face of the neck of the fusion pore, (d) by introducing positive curvature into the LE/L derived membrane patch during exocytosis, to form an inside-out vesicle in the growing TVS (e).

Table 1

Co-localization of MLN1-GFP staining with LysoTracker Red in lysosomes of fibroblasts

Transfected host cell	Construct	Percent co-localized
MLIV	pcDNA	N/A
	WT-MLN1-GFP	91.1 +/−2.0
	SL-MLN1-GFP	83.6 +/−7.0
	L106P-MLN1-GFP	79.7 +/−0.9
	F465L-MLN1GFP	80.2 +/− 2.8
Normal	WT-MLN1-GFP	77.0 +/−2.3